Collision-Energy Dependence of the Uptake of Hydroxyl Radicals at Atmospherically Relevant Liquid Surfaces

Collision-Energy Dependence of the Uptake of Hydroxyl Radicals at Atmospherically Relevant Liquid Surfaces

*Robert H. Bianchini, Maria A. Tesa-Serrate, Matthew L. Costen and Kenneth G. McKendrick**

Institute of Chemical Sciences, School of Engineering and Physical Sciences, Heriot-Watt University, Edinburgh, UK.

* E-mail: K.G.McKendrick@hw.ac.uk

ABSTRACT

A new experimental approach to the study of collisions of hydroxyl radicals with liquid surfaces is described, incorporating a molecular–beam source of OH (or, in practice, OD, for technical reasons) radicals. This allowed the collision-energy dependence of the scattering to be examined. The incident and scattered OD molecules were detected by laser-induced fluorescence. The representative branched, long-chain alkane, squalane (2,6,10,15,19,23-hexamethyltetracosane), and its partially unsaturated analogue, squalene (2,6,10,15,19,23-hexamethyl-2,6,10,14,18,22-

tetracosahexaene), were compared with perfluoropolyether as an inert reference liquid. Dynamical aspects of the scattering necessary to quantify the OD survival probability, and hence its complement, the reactive sticking coefficient, were determined. Results were obtained at average laboratory-frame kinetic energies of 7.2 and 29.5 kJ mol^{-1}; they are compared with previous independent measurements using a photolytic source of OH with an average kinetic energy of 54 kJ mol^{-1}. At lower collision energies, the survival probability is significantly lower on squalene than on squalane, but increases significantly with collision energy. This is consistent with a negatively-activated contribution to loss of hydroxyl through addition to double-bond sites at the squalene surface. In contrast, survival on squalane surface is found to be approximately independent of collision energy across the range examined. This is surprising, because it does not reflect the positively activated behavior typical of gas-phase OH + alkane reactions. We suggest that this may be explained by a higher probability of trapping dynamics at lower collision energies, enhancing the probability of reaction following migration to more reactive sites. The results have implications for the modelling of OH uptake on atmospheric aerosol surfaces as a function of chemical composition and temperature.

Introduction

The study of energy transfer and reactions occurring at the gas-liquid interface is important to improve the fundamental understanding of a wide range of technological and scientifically significant processes, such as respiration, distillation, combustion and atmospheric chemistry. Of particular relevance to this paper are the reactions of OH radicals with organic surfaces. As the predominant daytime atmospheric oxidant,[1] OH radicals are involved in many homogeneous and heterogeneous reactions, such as with volatile organic compounds (VOCs),[2] and the surfaces of atmospheric aerosols.[3-4] These interfacial reactions have been shown to alter the properties of the surface layer. The chemical 'ageing' towards a generally more oxidized and polar composition makes them more effective as cloud condensation nuclei.[2, 5-8] These changes in turn affect their optical properties, altering their contribution to radiative balance. Both the physical and chemical changes therefore have an effect on climate. There has also been recent interest in the role of elementary interactions of OH in other contexts, such as reactions with the antioxidants in the epithelial lining fluids and more generally as one of the most potent reactive oxygen species produced endogenously.[9]

To better understand its potential significance in the atmosphere, many measurements of the reactive uptake of OH at surfaces that mimic the organic component of aerosols have been made. This field, and related processes involving the atmospheric oxidants O_3 and NO_3, has been reviewed recently by Morris *et al*.[8] Proxy surfaces studied include liquid surfaces, waxes, self-assembled monolayers (SAMs), and sub-micron particles. The reactivity of OH on the surfaces is usually quantified by an uptake coefficient, γ, defined as the probability of reaction per collision with the surface.[10-11] The uptake coefficient can be obtained either by measuring the loss of OH directly,[12-18] or by measuring a change in the concentration of a species present at the surface.[8,

[19-27] Uptake coefficients obtained via the latter method have been known to produce values greater than unity, which is possible only through sequences of secondary reactions. The recent work of Wilson and coworkers[11] on squalane aerosols has shown that, in general, the measured uptake coefficient is an emergent property that reflects the net result of a sequence of elementary steps involving sticking, the initial abstraction reaction, and secondary radical reactions. Consequently, its value depends upon particle size, viscosity and OH concentration. The unique feature of the work that we present here, which is an extension of an approach we have developed previously,[15-16] is that it involves direct observation, in isolation, of the OH survival probability in the primary elementary encounter of OH with a liquid surface.

The majority of such fundamental, dynamical studies in this field have focused on inelastic scattering of atoms and molecules from liquid surfaces and closely related SAMs.[8, 28-29] This area has been pioneered by Nathanson and co-workers,[29] using projectile beams of atomic and molecular species coupled with mass-spectrometric detection. This method provides information on the energy transfer to the surface and the angular distribution of the scattered species, from which the scattering mechanism and aspects of the surface properties can be inferred. A related methodology was later developed by Minton *et al*.[28, 30] to study the products of reactions of the incident species with the surface, using a unique laser-detonation source capable of producing high-kinetic-energy atomic projectiles. A more limited number of studies have focused on analyzing the internal energy distributions of the scattered species using spectroscopic methods. Laser-induced fluorescence (LIF) was first used by McCaffrey *et al*. to study the inelastic collision of I_2 with surfaces.[31-32] In our own group, we have developed and applied this method extensively to the detection of OH radicals, both as a product of the reaction of $O(^3P)$ and $O(^1D)$ with hydrocarbon liquids,[33-43] self-assembled monolayers[44-45] and ionic liquids,[46-49] and from

inelastic scattering of OH itself from reactive and inert surfaces.[14-16] Nesbitt and coworkers have also recently used LIF to detect NO scattered from ionic liquids,[50-51] complementing their more extended earlier work using IR-laser absorption spectroscopy to study inelastic scattering, particularly of CO_2,[52-55] from a range of different liquids, and reactive scattering of F atoms at a hydrocarbon surface.[56-57]

One of the general features that has emerged from this body of work is that both inelastically and reactively scattered products can be characterized empirically as resulting from a combination of two limiting mechanisms. This will prove useful again in the interpretation of our new experimental results here. The first is a direct impulsive scattering (IS) mechanism, in which the scattered species leaves the surface with high translational energies and angular distributions correlated with the incident angle. The other is a thermal desorption (TD) mechanism, where the scattered species have a Maxwell-Boltzmann distribution of speeds and a $cos(\theta)$ angular distribution about the surface normal. These characteristics are consistent with molecules being trapped at the liquid surface long enough for them to be thermally accommodated before desorbing. However, dynamical scattering calculations[58-63] caution against the conclusion that all slower molecules have been formed from full trapping-desorption at the surface. While fast, directed products must certainly have been the result of a small number of relatively direct encounters, calculations predict that the slower molecules can be obtained from a range of interactions spanning single collisions through to the large number of encounters sufficient for full thermalization.

In our previous related investigations of OH scattering, the radicals were generated via photolysis of a precursor molecule at a short distance from the surface (typically 9 mm), and the scattered molecules were detected via LIF at the same distance. Photolysis of HONO[14-15] at 355

nm gave incident OH with a near-thermal rotational distribution and a substantially superthermal translational distribution; the average laboratory-frame kinetic energy, $<E_k>$, was 54 kJ mol^{-1}. This combination was particularly well-suited to the detection of the ballistic translation-to-rotation transfer expected in IS-type scattering. The OH was scattered off a number of potentially reactive liquid surfaces, including the widely used saturated hydrocarbon, squalane (2,6,10,15,19,23-hexamethyltetracosane), its partially unsaturated analogue, squalene (2,6,10,15,19,23-hexamethyl-2,6,10,14,18,22-tetracosahexaene), and oleic acid ((9Z)-octadec-9-enoic acid), with perfluoropolyether (PFPE) used as an inert reference. In particular, it was apparent that OH uptake was modestly but unambiguously enhanced on squalene relative to squalane; the reactivity on oleic acid was marginally suppressed relative to squalane.[15] With allyl alcohol as an alternative precursor, photolyzed at 193 nm,[16] the in-going OH radicals had a very hot rotational distribution (~2000 K), and broadly similar but somewhat higher translational energies ($<E_k>$ = 70–80 kJ mol^{-1}).[64-65] This complementary combination was chosen to enable the successful isolation of the TD channel, because of the substantial rotational relaxation that is required to populate the lower levels that dominate a thermal distribution.[16]

The significant advance we describe in this paper is the development of a new experimental set-up where OH radicals (or, in practice, OD for technical reasons that are explained below) are generated in a molecular beam, via a pulsed direct-current (DC) discharge. Conceptually similar sources have been shown previously to be capable of producing high OH number densities, rotationally cold species (with temperatures lower than 100 K), and small temporal and velocity spreads.[66-69] These attributes are highly advantageous in the current work, in which the pulsed OD beam is directed at normal incidence towards squalane, squalene and PFPE liquid surfaces and the scattered OD is detected by LIF. Crucially, the molecular-beam source allows the speed

of the in-going species, and thus the collision energy with the surface, to be adjusted in a controllable fashion through the choice of carrier gas. This contrasts with the previous photolytically based experiments described above where the collision energy was a fixed feature determined by the choice of precursor and photolysis wavelength; in practice, the available convenient combinations result in substantially superthermal translational energies. We study here the effect that changing the collision energy has on OD uptake at the liquid surfaces. Importantly, we access, for the first time, lower energies that approach more closely those that are relevant to uptake under atmospheric conditions. In the process, we uncover new information on the collision-energy dependence of the scattering dynamics of rotationally cold incident OD radicals from these liquid surfaces, but confine discussion here primarily to those features that are relevant to the correct interpretation of the uptake measurements.

Experimental approach

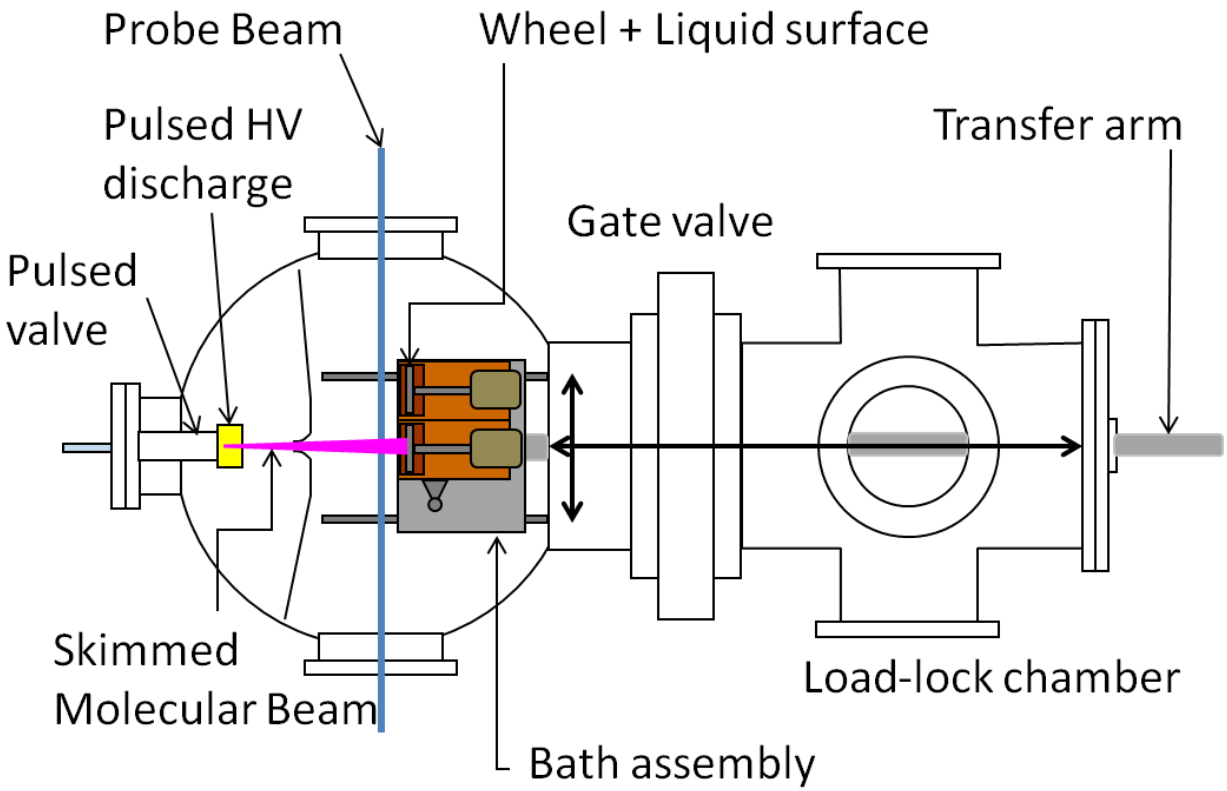

Figure 1: Plan overview of the experimental chamber, including the translation stage for the twin-liquid-bath assembly, and the load-lock chamber. The light-collection optics and PMT detector project vertically outward above the intersection point of the probe-laser beam and molecular beam; they are omitted for clarity.

The new apparatus designed to study translational energy-dependent collisions of unstable radicals with liquid surfaces is shown schematically in Figure 1. The essence of the method is to create a pulsed molecular beam of the projectiles, in this case OD radicals, which collide with a liquid surface at normal incidence. A pulsed probe laser beam intersects both the incident beam and the scattered molecules, which may be resolved in time. This allows the relative densities of

scattered and incident molecules to be measured accurately, and hence the survival probability (or its complement, the uptake) to be determined.

In practice, the apparatus consisted of two connected custom-made stainless-steel vacuum chambers: the main scattering chamber, where detection of the incident and scattered OD radicals was performed; and a load-lock chamber, into which the twin-liquid-bath assembly could be retracted and isolated from the main chamber via a gate valve. This allowed the load-lock chamber to be vented (with a dry N_2 purge, to minimize ingress of water vapor) and the liquids in the baths to be changed, without also venting the main chamber. This also had the added advantage that molecular-beam characterization could be performed in the absence of liquid surfaces. The main and load-lock chambers were kept under vacuum by turbomolecular pumps (Edwards STP-A1303C and STP-301, respectively), backed by dry rotary pumps (Edwards XDS 35i and XDS 10, respectively), which generated base pressures of ca. 10^{-6} mbar. The pressure in each chamber was monitored by a separate Penning-type gauge (Edwards WRG-S-DN40CF). The measured steady-state pressure in the main chamber with the molecular-beam valve operating was typically of the order of 1-3 x 10^{-5} mbar. This would be easily sufficient to ensure "nascent" detection conditions in which the mean free path exceeded the distances travelled by incident and scattered molecules. However, this does not account for the transient nature of the gas load. The absence of significant attenuation of the incident beam on introduction of the liquid surface (see below) is further reassurance that the effect of secondary gas-phase collisions was negligible.

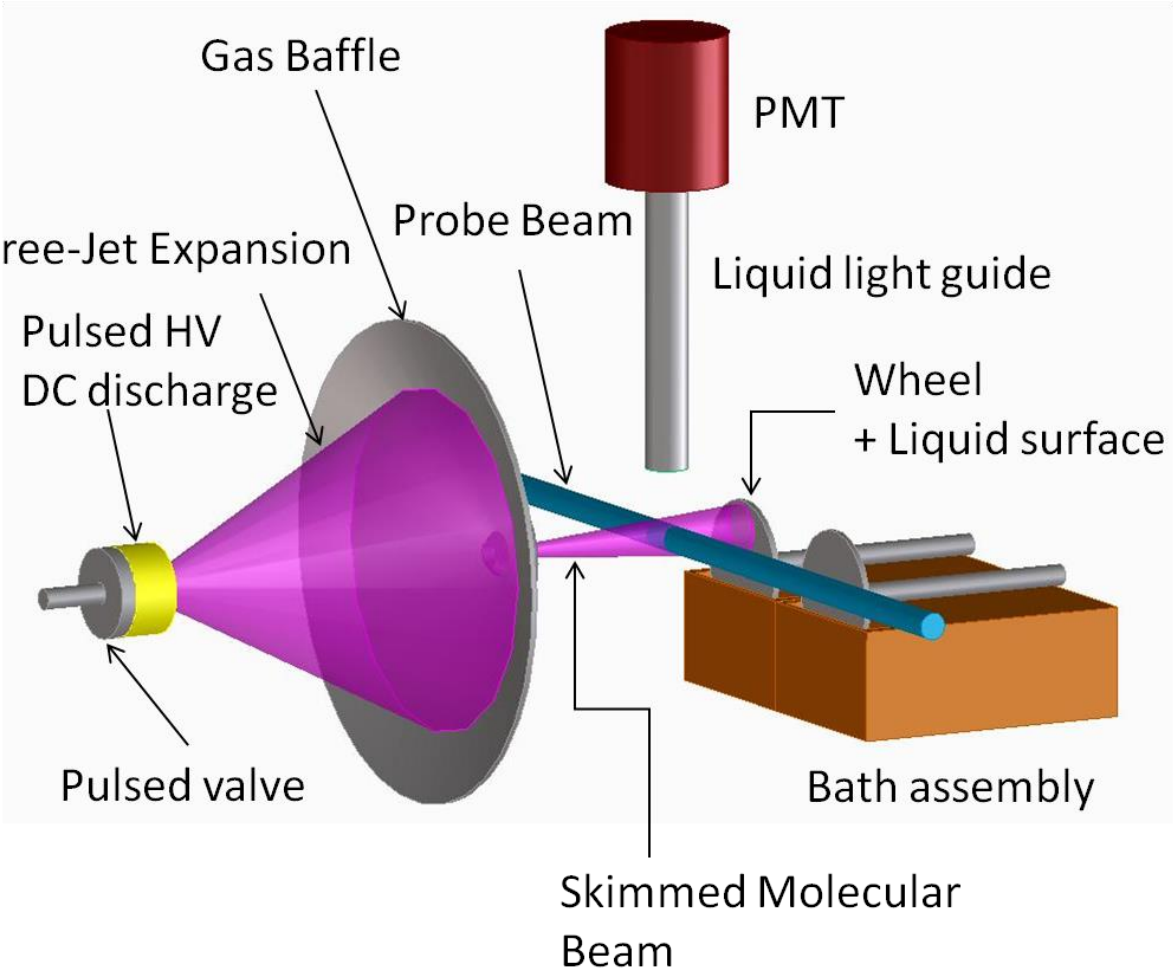

Figure 2: Schematic expanded view of the main scattering chamber, showing the geometry of the molecular beam and probe-laser beams. Objects are not necessarily drawn to scale. The molecular beam only scatters from one liquid-covered wheel at a time, as explained in the text.

The liquids of interest were contained in a pair of copper baths, mounted in a side-by-side arrangement, as indicated in Figure 1and in more detail in Figure 2. Each bath had a 5-cm-diameter stainless steel wheel that was partially submerged in a trough of the liquid. The wheels rotated at 0.5 Hz, becoming coated by a constantly refreshed layer of liquid. The whole bath assembly could be translated in the direction perpendicular to the molecular beam while retracted

into the load-lock chamber. Consequently, when engaged in the scattering chamber, only the selected bath was in line, at normal incidence, with the molecular beam. This allowed two different liquids to be studied in back-to-back measurements without venting the chamber, providing a direct comparison between scattering from different surfaces. The entire assembly was translated in the direction parallel to the molecular beam via a mechanical arm. As well as providing the means for complete retraction into the load-lock chamber, this allowed the distance between the active wheel and the probe beam to be set precisely in the scattering chamber. In all the experiments reported here, this distance was 10 ± 1 mm. The error reported accounts for possible variations in the exact position of the surface due to repeated translation of the bath assembly between experiments.

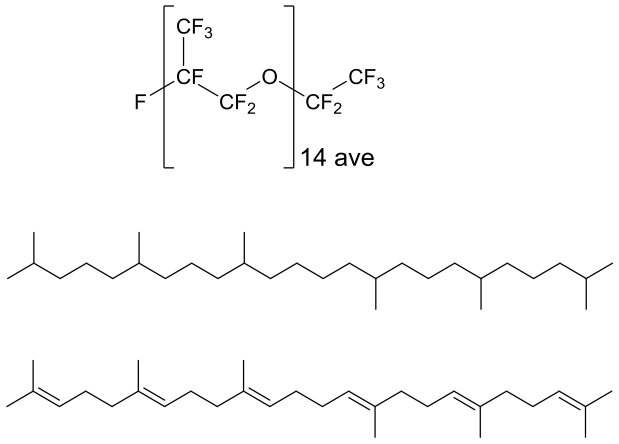

Figure 3: Molecular structures of the liquids investigated: PFPE (top), squalane (middle), squalene (bottom)

The liquids investigated were the saturated hydrocarbon squalane and its unsaturated counterpart squalene (both sourced from Aldrich), and PFPE (Krytox® 1506 (F-$[CF(CF_3)CF_2O]_{14ave}$-CF_2CF_3) sourced from DuPont). PFPE was selected as an inert reference liquid, as previously[14-16] and explained further below. All three liquids have vapor pressures that

are sufficiently low (~10^{-7} mbar at room temperature) to make them compatible with use under vacuum. The chemical structures of these liquids are shown in Figure 3.

Hydroxyl radicals were produced by pulsed electrical discharge in an expansion of water vapor in an inert carrier gas. In practice, D_2O was used as the precursor, generating OD radicals. This was a precaution against the possibility of production of OH at the hydrocarbon liquid surfaces via processes other than simple inelastic scattering of the incident OH. Given the absence of O atoms in the structure of either squalane or squalene, no such issue could arise from the generation in the discharge of H atoms, either in the ground or conceivably metastable (or even ionized) states. However, O atoms, or metastable species containing O, could have been problematic. In particular, it is known from extensive previous work that ground-state $O(^3P)$ reacts with squalane and squalene at moderate collision energies to produce OH.[30, 34-36, 38-40, 43] The use of OD as the incident projectile avoids any possible contamination of the desired inelastically scattered signal by that resulting from this unwanted side reaction. We do not anticipate significant isotope effects in the uptake of OD versus OH at these liquid surfaces, because breaking or even extension of the existing O-H/D bond does not correspond to the reaction coordinate for either H-abstraction or OH-addition reactions (see below). A 10-20 mL sample of D_2O (99.9% purity, Cambridge Isotope Laboratories, Inc.) was placed in a stainless steel T-piece containing a flat-bottomed glass tube. A gas line, capped with a blank top with a 0.5 mm aperture drilled in it, was connected to the T-piece so that the cap is fully submerged. The carrier gas (He or Ne, BOC gases, CP Grade, 99.999% purity) was bubbled through the D_2O reservoir using a high pressure of carrier gas (3 bar of He and 2 bar of Ne). Assuming the equilibrium vapor pressure is achieved, this provides mixtures of ≈1% and ≈1.5 % D_2O in He and Ne, respectively.

The gas mixture was fed to a pulsed valve (General Valve, series 9) with a 1.0 mm aperture. This was fitted with a custom-built, pulsed-electrical-discharge device, based on a design developed by Ikejiri *et al.*[67] It consisted of a pair of electrodes, insulated from each other and from the faceplate of the valve via Teflon spacers. A pulsed, negative DC voltage was applied to the front electrode (furthest from the valve), with the other electrode grounded, resulting in a barrier discharge when coincident with the gas pulse. This polarity ensures that electron flow counter-propagates the direction of travel of the molecular beam, which has been shown to provide a more stable discharge.[70] The high voltage was supplied by a power supply (Bertan model 353) connected to a fast switch (DEI PVX-4140). This was triggered externally to switch between ground and the optimized voltages of -1400 V for the He-seeded beam and -1150 V for the Ne-seeded beam in a 10 μs pulse, timed to fire typically 100 μs into a gas pulse of nominal overall length 500 μs. The voltages were established by monitoring the density of OD generated (see below) while ensuring the stability of the supplied-current waveform.

The free-jet expansion was collimated by a 5 mm diameter conical skimmer located 167 mm from the valve nozzle and 160.5 mm from the last constraining element of the discharge device, i.e. the aperture of the front electrode. The transmitted molecular beam was intersected at right angles by the probe-laser beam 230 mm from the valve nozzle. A gas baffle formed from aluminum foil was attached to the plate on which the skimmer was mounted to effectively divide the main chamber into separate source and scattering chambers. This reduced the gas load in the scattering chamber in the vicinity of the target liquid-covered wheel. It also successfully prevented OD radicals that did not pass through the skimmer from reaching the probe region, during the time period of interest, via indirect trajectories involving scattering from the surfaces of components in the chamber or secondary collisions in the gas phase.

The use of such a source ensures that the liquid surface receives a very low total dosage of gas, particularly by potentially reactive species. We illustrate this in outline here; further details are given in the Supporting Information (Section 1). The flux from an essentially identical valve has been independently characterized experimentally, including with He as the carrier gas and spanning the backing pressures that we use here.[71] (We focus on a He beam for the purposes of illustration, but similar considerations apply to Ne as the carrier.) With straightforward and minor adjustments for the respective distances from the source, this implies a peak total gas number density at the point where the molecular beam intersects the liquid surface in our experiments of ~2×10^{14} cm^{-3}; this is in line with the general expectation for pulsed molecular-beam sources.[72] Combined with the measured average He beam speed (see below), the total flux at the liquid surface is ~3×10^{19} cm^{-2} s^{-1}.

For the purposes of this illustration, we take a surface site to be an individual C atom and its associated H atoms. There are a number of ways of estimating the areal density of these sites at the squalane or squalene surface (see Supporting Information (Section 1) for details) but they all suggest a value within small factors of ~1 x 10^{15} cm^{-2}.

Considering first the stable species present in the molecular beam, the incident flux is present at the surface for ~100 μs before the probe pulse. The total dosage of the surface is therefore ~3 $\times 10^{15}$ cm^{-2}, or around 3 per surface site. However, the great majority (99% - see below) of this is He. The very low binding energy of He (or Ne) to a hydrocarbon surface ensures that the lifetime for desorption is assuredly sub-ps, so no significant accumulation of the bulk carrier gas will occur.[73] Even for H_2O (or D_2O) for which a reasonable estimate of the binding energy is the inverse of the solvation enthalpy of -17 kJ mol^{-1},[73] the predicted lifetime for the subset of trajectories that undergo trapping-desorption is still only ~0.1 ns. Some corroboration of this

estimate comes from direct observations of HCl scattering from cold salty water,[74] or of D_2O itself from a more strongly interacting, polar organic (nopinone) film.[75] In both cases, despite the stronger binding than for D_2O with squalane or squalene, measured residence times are below the experimental resolution of ~1 or ~10 μs, respectively. The steady-state coverage during the gas pulse is therefore a negligible fraction of the already small proportion of ~3% of surface sites if every D_2O molecule (present at a 1% mixing ratio – see below) stuck permanently to the surface.

Any remaining realistic possibilities responsible for any secondary chemistry must therefore result from reactive species formed during the discharge. Previous independent work has shown that the ratio of He metastable species to ground-state He in similar pulsed-discharge molecular beams is in the range 10^{-7} - 10^{-5}.[76-78] The proportion of surface sites that could be modified by metastable He is therefore a similar negligible fraction of the ~30% that could in principle react during the ~10 μs of the gas flow for which the discharge is on, even ignoring diffusion away from the surface (see below). A more plausible candidate is perhaps the intended OD projectile, or other fragments formed from the dissociation of D_2O. The efficiency of dissociation under our conditions is not known accurately, but previous related studies have suggested 10 – 100%.[66] Taking the absolute upper limit of 100%, the dosage would correspond to ~0.3% of a single layer of surface sites. This is already probably safe enough to be neglected, but also ignores the effects of diffusion during the timescale of the dosage with reactive fragments. Self-diffusion coefficients for squalane are known accurately;[79] those for similar-sized reaction products in squalane (or squalene) can reasonably be assumed to be similar. As we show in detail in the Supporting Information (Section 1), the average distance, $\langle z \rangle$, that such species will diffuse in an interval, τ, in the normal direction away from the liquid surface in the ~10 μs for which

reactive species are incident is ~200 Å. This is more than ten times the average squalane end-to-end distance of 18 Å, as determined in MD simulations.[37] Put the other way, on average, the time required for molecules to diffuse to a depth of greater than one molecular layer is ~100 ns. Therefore the steady-state fraction of exposed sites which have undergone reaction is reduced by around another two orders of magnitude below the ~0.3% estimate above. This further reinforces the conclusion that each incident OD radical interacts individually with an essentially unmodified surface layer; any secondary chemistry involving encounters between more than one species in the beam or their reaction products is very safely negligible under these conditions.

The probe pulse for LIF was produced by a dye laser (Sirah Pulsed Dye Laser, CSTR-LG-24) pumped by a Nd:YAG laser (Continuum Surelite II-10). Second-harmonic generation was used to obtain the required wavelengths in the UV region. The probe beam had a diameter of 3 mm and was horizontally polarized. It passed through the center of the main scattering chamber, via a set of internal circular baffles designed to reduce the detection of scattered laser light or the fluorescence background that was found from some liquid samples if irradiated by the diffraction halo of the probe beam.

LIF was excited on the well-known OD A-X (1,0) band. Pulse energies were kept constant by learning a suitable tuning curve for the doubling crystal across the relevant wavelength range (287 – 289 nm) and set at ~200 μJ/pulse using a combination of a polarizer and a λ/2 waveplate. The fluorescence was collected by a liquid light guide (Ultrafine Technology Ltd. Series 300, length 500 mm, diameter 8 mm), placed 20 mm above the intersection of the probe laser and molecular beams. A dichroic filter, centered at λ = 317 nm with FWHM = 8 nm (Laser Components) were used to isolate emission on the A-X (1,1) band and further reject scattered probe-laser light. The transmitted light was detected by a photomultiplier tube (PMT) (EMI,

9813QB). The signal from the PMT was captured by an oscilloscope (LeCroy Wavesurfer 434, 2 Gigasamples/s, 350 MHz bandwidth) interfaced to a personal computer. This also controlled, via custom-written LABVIEW® software, the probe laser wavelength and a delay generator (BNC 565) which synchronized the triggering of the pulsed valve, the probe laser, and the pulsed DC discharge. The experiment operated at a frequency of 10 Hz.

The experiments reported in this paper fall into two basic types. The principal data were *time-of-flight (TOF) profiles*, acquired by varying the delay between the high-voltage discharge pulse (synchronized to the gas pulse) and the probe-laser pulse, with the probe laser tuned to a particular OD rovibronic transition. This provides information on the speed (and hence translational energy) distributions of both incident and scattered OD. With appropriate normalization, the intensities of the TOF profiles taken on different transitions also provide relative populations in different product rovibrational states. *Excitation spectra*, on the other hand, were acquired by scanning the wavelength of the probe laser at a fixed discharge-probe pulse delay; they give information on the internal-state distribution of OD at that delay. As explained below, in the current work these were used mainly for characterization of the internal-state distribution of the incident beam and as corroboration of the scattered populations derived from TOF profiles.

The incident beam was characterized prior to collisional experiments with the surfaces. The liquid-bath assembly was fully retracted into the load-lock chamber during these measurements. TOF profiles taken on the $Q_1(1)$ transition provided information on the measured average velocity of the OD packet and its spread of speeds. The OD rotational distributions in the incident beam were characterized by recording excitation spectra at the peak of the TOF profiles of the incident beam for the two different carrier gases. In both cases, the TOF profiles of the

incident beam are close to Gaussian, with a full-width-at-half-maximum (FWHM) of 17.5 ± 0.3 μs for the He carrier and 45.8 ± 0.4 μs for the Ne carrier. The average speed of the OD radicals is 1811 ± 8 m s^{-1} with the He carrier and 894 ± 3 m s^{-1} with the Ne carrier; these correspond to average laboratory-frame kinetic energies, $\langle E_k \rangle$, of 29.5 ± 0.3 kJ mol^{-1} and 7.20 ± 0.06 kJ mol^{-1}, respectively. For both carriers, the OD rotational distribution has the majority of the population in the lowest few N levels (45% in $N = 1$ and 28% in $N = 2$ with the He carrier; 48% in $N = 1$ and 18% in $N = 2$ for Ne), accompanied by a secondary hotter distribution extending to higher N. A standard Boltzmann analysis confirmed that the distributions were not well-described by single temperatures. Further details of the characterization are given in the Supporting Information (Section 2).

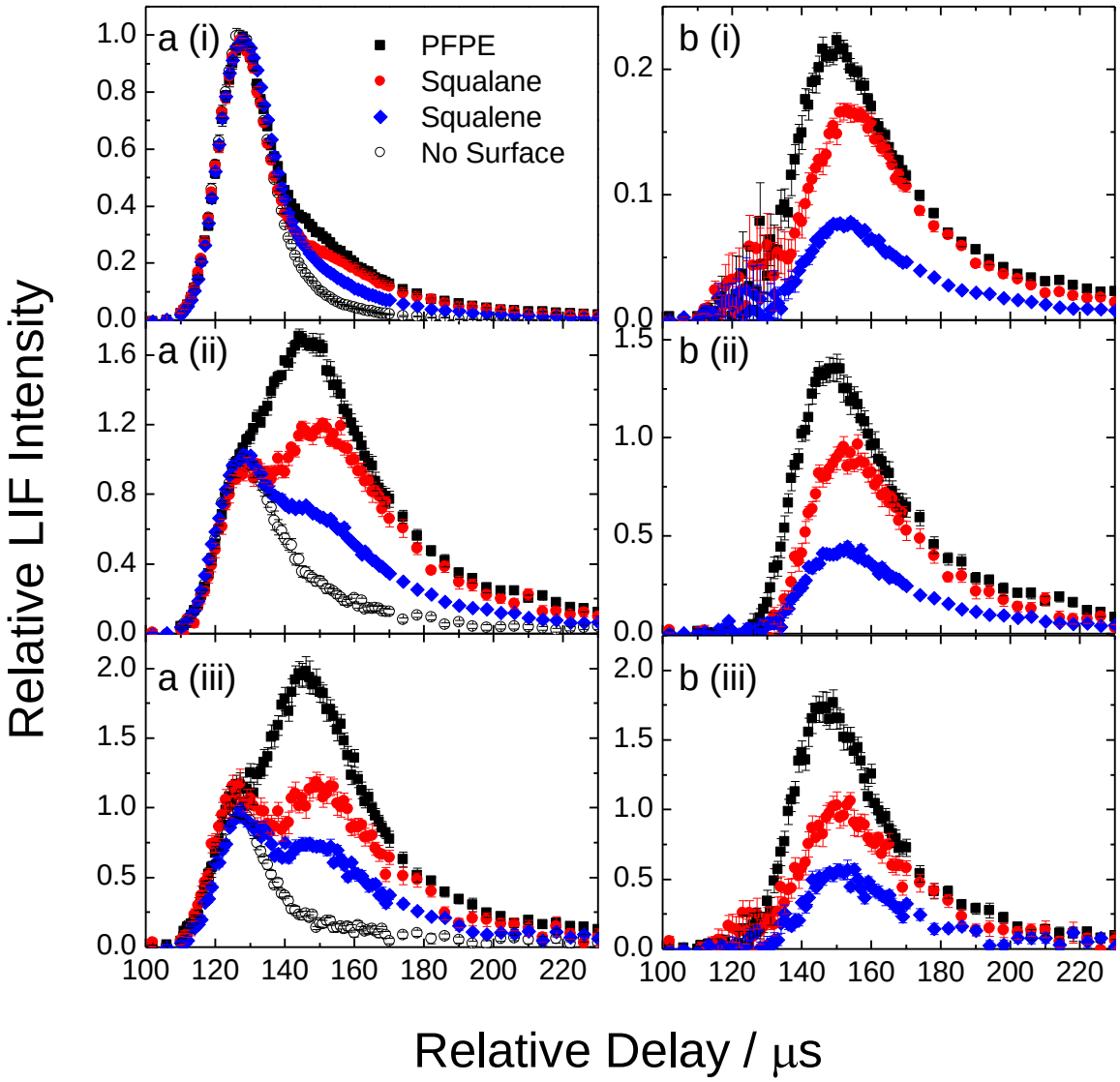

Figure 4: TOF profiles of the intensity of the OD A-X (1,0) LIF transition as a function of discharge-probe delay with $\langle E_k \rangle = 29.5 \pm 0.3$ kJ mol^{-1}. The incident beam with no liquid surface present is represented by open circles. The remaining profiles include scattered signals with a liquid surface at a distance of 10 ± 1 mm from the probe beam: PFPE (black squares), squalane

(red circles) and squalene (blue diamonds). (a) Raw profiles; (b) profiles following subtraction of the incident beam. Probe transitions: (i) $Q_1(2)$, (ii) $Q_1(5)$, (iii) $Q_1(8)$. All profiles have been normalized to the peak of the corresponding incident beam.

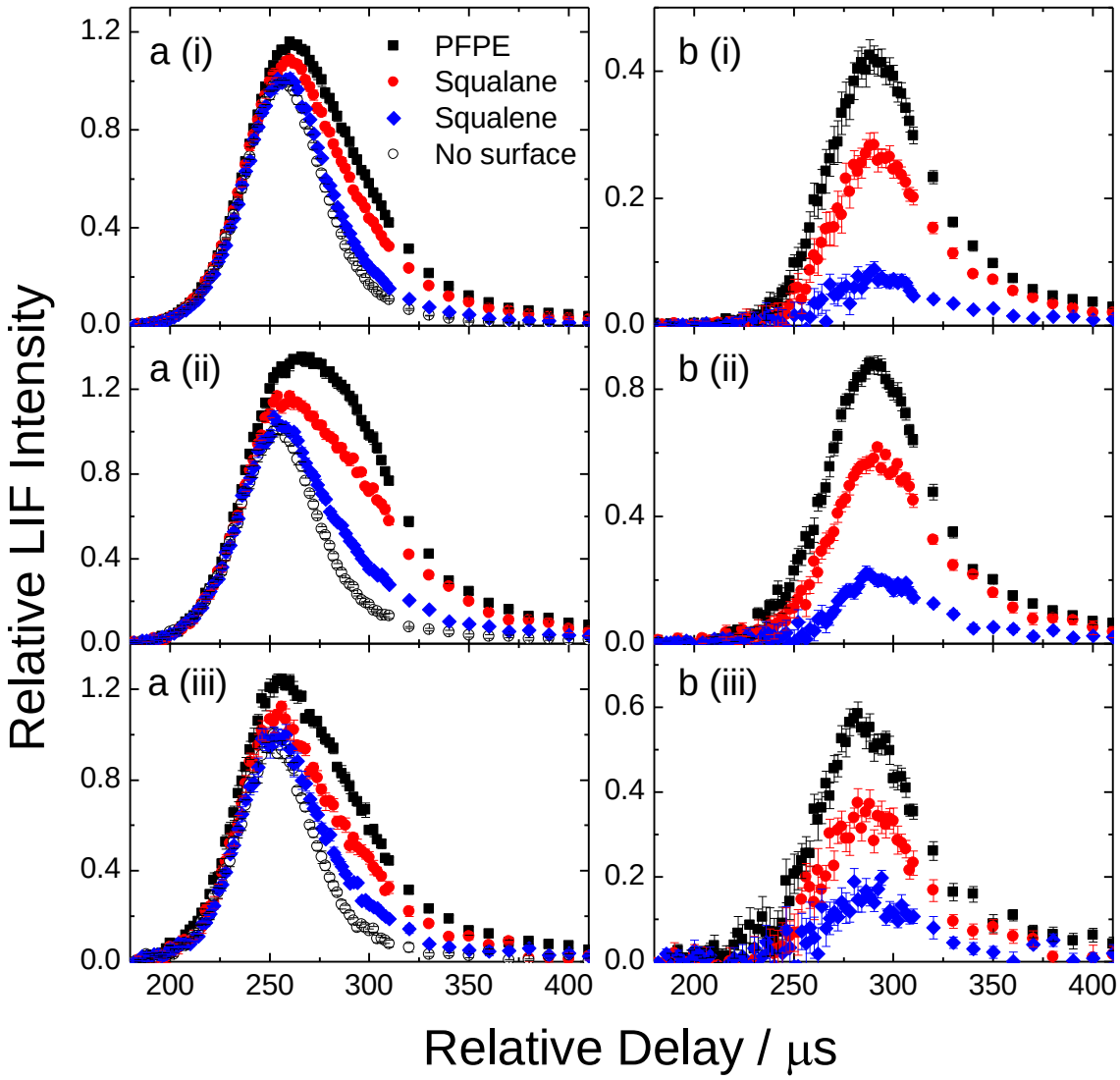

Figure 5: TOF profiles of the intensity of the OD A-X (1,0) LIF transition as a function of the discharge-probe delay with $\langle E_k \rangle$ = 7.20 ± 0.06 kJ mol^{-1}. The incident beam with no liquid surface present is represented by open circles. The remaining profiles include scattered signals with a liquid surface at a distance of 10 ± 1 mm from the probe beam: PFPE (black squares),

squalane (red circles) and squalene (blue diamonds). (a) Raw profiles; (b) profiles following subtraction of the incident beam. Probe transitions: (i) $Q_1(2)$, (ii) $Q_1(5)$, (iii) $Q_1(7)$. All profiles have been normalized to the peak of the corresponding incident beam.

Results

TOF profiles

Figure 4 shows the OD TOF profiles for each of the three liquids using He as the carrier gas. Figure 5 shows the corresponding TOF profiles taken with Ne as the carrier gas. The delays reported are relative to the start of the discharge pulse. The profiles were measured systematically via the $Q_1(2)$, $Q_1(5)$ and $Q_1(8)$ transitions with the He carrier, and via $Q_1(2)$, $Q_1(5)$ and $Q_1(7)$ with the Ne carrier. These transitions were chosen because they span, in approximately equal rotational energy increments, the range of N' levels significantly populated via collisions at the surfaces. The results displayed represent averages of between 9 and 12 individual profiles, with 30 laser shots per point, for each of the lines. A full set of profiles was acquired for the PFPE liquid alongside a set for squalane, alternating surfaces between each individual profile. A smaller set of PFPE profiles was acquired in conjunction with the full set for squalene, with individual PFPE profiles acquired at regular intervals between squalene profiles, thus ensuring reproducibility of the results.

The figures include representative TOF profiles of the incident beam probed on each transition, where the bath assembly was retracted into the load-lock chamber. Individual profiles of the incident beam were acquired alternately between profiles with the surfaces in place, to ensure

consistency of the incident beam intensity. The profiles in Figure 4 and Figure 5 were normalized to the average of all the incident beam profiles taken on the same day.

All the profiles with the liquid surfaces in place show clearly that additional OD signal is present at later times relative to the incident beam profile; this is obviously consistent with OD that has scattered and rebounded into the probe region. The inclusion of the skimmer and the gas baffle, as described in the experimental section, ensures that this additional OD can only come from collisions with the liquid surface and not with other parts of the bath assembly or via indirect routes from the source region. For most of the transitions, a straight subtraction of the daily-average incident beam profile from the raw profiles was sufficient to give a profile with no systematically unphysical residuals at early delays. The slight exception was the $Q_1(2)$ profile at the higher collision energy where the scattered signal is the lowest proportion of the incident beam. This suggests that there is some small attenuation of the incident beam, likely due to the OD radicals scattering from carrier gas that has rebounded from the surface prior to OD arriving in the detection region. In this case, the incident beam profile was scaled by an empirically determined factor, which was on average 96% of unity, and never smaller than 93%, to ensure the subtraction smoothly approached zero at early times, as physically required. .

From the point of view of the current work, the main features of interest in both Figure 4 and Figure 5 are the obvious systematic variations in the relative magnitudes of the scattered signals for the different liquids. The scattered signal is consistently largest for PFPE at either collision energy and across all transitions studied, and progressively smaller for squalane and then squalene. We quantify these differences below.

Although they are not the primary focus here, there are also clearly some interesting dynamical differences between scattering from the different liquids. We describe them only relatively

briefly here, focusing mostly on the features of the translational and rotational distributions of the scattered OD molecules which are necessary for the quantification of the desired integral survival probabilities. The scattered profiles obtained at higher $<E_k>$ in Figure 4 show a noticeable difference in the peak arrival times between the liquids, for all transitions studied. The peak from PFPE is always earliest, and from squalane the latest. However, in the profiles at lower $<E_k>$ in Figure 5, any such differences are not readily apparent. Comparisons between profiles from the same liquid taken on different transitions also show some subtle differences in shape. Figure 6 shows this comparison for the profiles from PFPE at both collision energies; similar differences are observed with the other liquids. At higher $<E_k>$ in Figure 6(a), the rising edges are relatively similar in all cases, whereas at longer times the profiles for $N' = 5$ and 8 decline progressively more rapidly relative to $N' = 2$. The behavior is generally similar, although less clear-cut, at lower $<E_k>$ in Figure 6(b): the slightly more rapid rise for the $N' = 7$ data may be an artifact of its lower signal to noise.

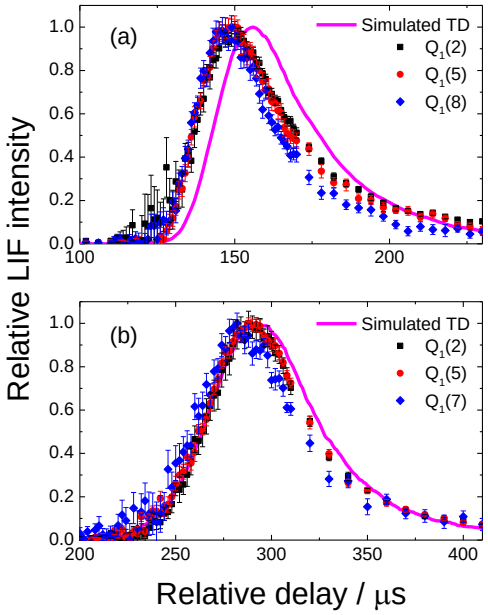

Figure 6: Peak normalized TOF profiles of the scattered OD from the PFPE surface on the discharge-probe delay, at (a) high and (b) low collision energies. Transitions probed are $Q_1(2)$ (black squares), $Q_1(5)$ (red circles), and $Q_1(7)$ [in (a)] or $Q_1(8)$ [in (b)] (blue diamonds). Solid lines represent a Monte-Carlo simulation of the anticipated TD profile (magenta), as described in the text.

Overall, there is a clear indication of some positive correlation between the translational and rotation energies of the scattered OD. This is related to the underlying dynamics of the scattering. Also shown for comparison in Figure 6, is a Monte Carlo simulation of the expected profile if all scattering occurred by a fully thermalized TD mechanism. The simulation was carried out on a similar basis to those which we have described previously,[35] accounting for temporal, spatial and speed distributions of the incident OD, but adapted for the change from the

photolytic to molecular-beam source. The translational energies of a significant fraction of the scattered products are clearly superthermal for collisions at higher $<E_k>$ in Figure 6(a), implying a considerable proportion of IS-like scattering. The situation is less clear at the lower $<E_k>$ in Figure 6(b), where the departure from the predicted TD distribution is marginal. It is probably not possible on this basis to distinguish contributions from a TD-like mechanism and IS scattering that happens to produce near-thermal final speeds because of the modest incident energy.

The results in Figure 6(a), in particular, also imply that both integration over the product speeds and summation over the internal state distribution of the scattered OD is necessary to assess correctly the survival probabilities. In principle, the same, complete information would be contained in sets of either excitation spectra recorded at a sufficiently closely-spaced set of delays, or TOF profiles measured on transitions probing every final quantum state. Either set of measurements would have to be performed with the liquid surfaces both present and absent, so that the incident contribution could be subtracted. In practice, either approach would have been impractically laborious, so a compromise was reached. It is more efficient to derive the rotational populations from normalized TOF profiles on selected transitions of the type shown in Figure 4 and Figure 5. This avoids the inherent drawback of the excitation spectra approach that the majority of the acquisition time is spent collecting data away from the peaks of the transitions. Analysis of the excitation spectra is also subject to larger statistical errors because of the need to subtract a correctly weighted, but significant, contribution from the incident beam that is, in general, still present during the peak region of the scattered profile. Therefore, we report in the main text here the results from the normalized TOF profiles. Nevertheless, we recorded some selected excitation spectra at the peaks of the TOF profiles to provide corroboration. Details of

the spectra and their analysis are provided in the Supporting Information (Section 3). The results are generally in reasonable agreement with those derived from the TOF profiles and would not imply any qualitatively different conclusions.

To extract product rotational distributions from TOF profiles (or excitation spectra), it is necessary to compensate for any systematic factors, such as partial optical saturation and wavelength-dependent variations in probe pulse energy, which potentially affect the conversion of intensities to populations. Phenomenological calibration factors were derived experimentally by recording the spectrum of a fully thermalized sample of OD, similar in principle to the method described in our previous related work.[35] The thermalized sample was generated in this case by operating the electric discharge with a static high voltage; this produced a high integral yield of OD by effectively dissociating D_2O throughout the ~ 500 μs of the gas pulse. Spectra were collected at a very long delay of ca. 5 ms, where the residual OD can very safely assumed to be thermalized. The apparent populations extracted from these spectra using the LIFBASE spectral simulation program[80] gave very good fits to Boltzmann temperatures that were always within ~20 K of the true laboratory temperature of 296 K. The ratios of these populations to those of the known thermal distribution at the laboratory temperature were used to derive the line-dependent correction factors; the departure from unity was generally less than 10% and in no case larger than 17%.

We have described the basic approach to the derivation of global (i.e. integrated over the full TOF profile) rotational populations from TOF profiles in previous papers.[15] The distributions were obtained by integrating the profile from each liquid on each transition. The scattered profiles were integrated from 135 μs to 230 μs delay at high collision energy, and from 250 μs to 410 μs at low energy. The lower limits were chosen to avoid integrating over the noisy baseline

region at early times, which is subject to the largest errors caused by subtraction of the incident beam. The integral yields, after applying the thermal calibration corrections discussed above, were used as three points in a Boltzmann analysis. There is no fundamental reason, of course, why the results of dynamical, IS-like scattering should be well-described by a single temperature, but in general the 3-point fits were reasonably linear; details of the Boltzmann fits are given in the Supporting Information (Section 4). The resulting temperatures are listed in Table 1.

Table 1: Rotational temperatures, T_{rot}, of scattered OD radicals derived from integrated TOF profiles.

	T_{rot} / K	
Liquid	He carrier; $\langle E_k \rangle = 29.5 \pm 0.3$ kJ mol^{-1}	Ne Carrier; $\langle E_k \rangle = 7.20 \pm 0.06$ kJ mol^{-1}
PFPE	401±19	297±14
Squalane	390±18	304±16
Squalene	419±21	335±30

It is clear from Table 1 that the major influence on the rotational excitation of the scattered OD is the incident kinetic energy. All the rotational temperatures at the higher $\langle E_k \rangle$ are of order 100 K higher than thermal, whereas at the lower $\langle E_k \rangle$ they are generally closer to thermal. Squalene may be something of an exception, giving the highest temperature at both collision energies; this may have a dynamical explanation, as we discuss below.

OD loss at the liquid surface

Our experimental approach measures directly the fraction of OD that survives an encounter with the liquid surface. Given the discussion above (see Experimental approach) of the very low dosage of the surface, this reflects only the primary process of direct reaction of OD with unmodified squalane or squalene molecules. We quantify this fraction in terms of a survival probability, σ, which we define in terms of the ratio of the integrated product density from a potentially reactive liquid, $D(N')_{liq}$, to that from PFPE, $D(N')_{PFPE}$, in a specific final rotational state, N'. For the integrated densities to correctly represent the total populations across all final rotational levels, they must be adjusted for the relative fraction of the total rotational populations, $p(N')_{liq}$ and $p(N')_{PFPE}$, that resides in the level for which the profiles were measured:

$$\sigma = \frac{\int_{t_{min}}^{t_{max}} D(N\prime)_{liq} dt}{\int_{t_{min}}^{t_{max}} D(N\prime)_{PFPE} dt} \times \frac{p(N\prime)_{PFPE}}{p(N\prime)_{liq}} \qquad (1)$$

For reasons described in the previous section, we restrict the integration of the TOF profiles from Figure 4 and Figure 5 to $t_{min} \geq 135$ μs for the higher $\langle E_k \rangle$, and $t_{min} \geq 250$ μs for the lower. We also use the $p(N')$ fractions that are determined from the T_{rot} values in Table 1 derived from the TOF profiles. (These are by construction more representative of the integrated population distributions over all times than excitation spectra measured at a single delay).

Following the definitions of Houle *et al.*,[11] the survival probability is assumed to be simply the complement of the sticking coefficient, S, i.e. the fraction of incident molecules that are not elastically or inelastically scattered and do not redesorb without reaction:

$$S = 1 - \sigma \qquad (2)$$

As discussed at length in the atmospheric chemistry literature, this is related to, but not necessarily the same as, the reactive uptake coefficient, γ, introduced in the Introduction. This is also widely reported from other techniques.[8, 10-11]

Equation (2) assumes that loss of OD at the squalane or squalene surfaces is exclusively due to reaction. It is also assumes that there are no OD molecules lost at the PFPE surface through any process. We have used realistic Monte Carlo simulations of scattered TD profiles, to establish that this is a reasonable assumption, as explained in further detail in the Supporting Information (Section 5). In essence, this was based on the comparison of the magnitudes of the observed and TD-simulated scattered profiles, relative to the incident beam, for a given N'. Due account was taken of the known fractions of the incident and scattered populations in this level. The relative fluxes of incident molecules at the two different collision energies were obtained from their TOF profiles, which measure the density, corrected for their known average speeds. The simulation procedure correctly predicts relative densities of TD-scattered products. Reassuringly, for the lower $<E_k>$, for which it is known from Fig. 6(b) that a TD profile reproduces quite faithfully the shape of the observed profile, the predicted magnitude of the scattered profile almost exactly matched (within 5 %) the observation for $N' = 2$ from PFPE. The prediction was less perfect (peak density over-predicted by ~ 24%) at the higher $<E_k>$. However, the sense of this deviation is consistent with the known superthermal character of the observed distribution (Fig. 6(a)) which decreases the density for a given flux. We are unable to carry out a rigorous density-flux transformation to confirm this conclusion because it would require a full characterization of the scattered speed and angular distributions (which, unlike for an assumed TD distribution, is unknown *a priori*). Nevertheless, the approximate version that we also describe in the Supporting Information (Section 5) suggests that the reduced intensity at the higher $<E_k>$ is indeed accounted for adequately by flux-density effects.

For similar reasons, the survival probabilities that we derive via Equation (1) based on integrated densities will be relatively immune from any systematic effects of flux-density

conversion at the lower $<E_k>$, because the shapes of the profiles from all three liquids are very similar (Fig. 5(b)). At the higher $<E_k>$, there are subtle differences between the profiles from the different liquids; as noted, the OD scattered from squalane appears to have a slightly slower speed distribution than from PFPE or squalene. To take this properly into account would again require either untested assumptions or additional measurements significantly beyond those reported here, so we simply note that the survival probability for squalane may have been slightly over-estimated.

Table 2: Survival probabilities of OD from each liquid surface.

	Ne Carrier $<E_k>$ = 7.20 ± 0.06 kJ mol^{-1}	He Carrier $<E_k>$ = 29.5 ± 0.3 kJ mol^{-1}	Bulk photolysis[c] $<E_k>$ = 54 kJ mol^{-1}
PFPE[a]	1.00	1.00	1.00
Squalane	0.63±0.06[b]	0.68±0.04[b]	0.70±0.08[b]
Squalene	0.21±0.02[b]	0.31±0.02[b]	0.61±0.07[b]

[a]A survival probability of unity is assumed for PFPE.

[b] 1σ errors reflect the compounded effect of relative uncertainties in the magnitude of all contributing TOF profiles.

[c]From reference [15]

In principle, the survival probabilities derived from the TOF profiles would be the same for each of the observed product levels, N', for a given reactive liquid. However, this relies on the relative integral populations being described perfectly by the fitted value of T_{rot}. In practice, the finite scatter around the best-fit line in the Boltzmann analysis results in slight differences in the resulting survival probabilities. To take due account of this, the average of the individual survival

probabilities was taken, propagating individual statistical uncertainties in the results for each N' into the final uncertainty. These average survival probabilities are listed in Table 2, alongside the values previously obtained using the 'bulk photolysis' method which will be discussed further below.[15] Note that the relative survival probabilities between squalane and squalene are statistically better determined than might be immediately apparent from Table 2, because the uncertainties quoted depend on statistical fluctuations in the signals from each reactive liquid and in the PFPE profiles with which they are compared. This was also true in the previous photolytic experiments, where it was clear, for example, that the more modest differences in survival probability between squalane and squalene were systematically robust. The sticking coefficients for squalane and squalene, obtained by applying Equation 2 to their respective survival probabilities, are shown in Figure 7.

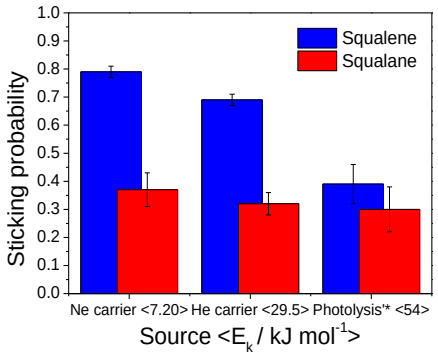

Figure 7: Sticking coefficients S for OD at the surfaces of squalane (red) and squalene (blue), in order of increasing collision energy. * From reference [15].

Discussion

The main aim of this paper was to demonstrate that the molecular-beam based approach could be used to measure the collision-energy dependence of OH (or OD) sticking coefficients on

different liquid surfaces, which we have done successfully. Some interesting information on the dynamics of scattering is also obtained. We discuss this briefly first, concentrating primarily on those aspects that are necessary to extract reliable sticking coefficients.

Dynamical information

As demonstrated above, OD scattered off surfaces at the higher collision energy with $<E_k>$ = 29.5 kJ mol^{-1} generally show superthermal rotational distributions, which are reasonably well described as Boltzmann temperatures. There are identifiable dynamical differences depending on the identity of the surface. The implication is that a significant amount of OD scatters off all the surfaces via an IS mechanism. This is broadly in agreement with previous measurements using photolytic sources of OH with somewhat higher collision energies.[14-16] The more efficient conversion of kinetic to rotational energy for PFPE than for squalane is consistent with well-established differences in the stiffness of these two surfaces with a range of gas-phase projectiles.[28-30, 33, 35, 44, 46, 52, 56, 81] The predominance of single-bounce, IS-type trajectories with some conversion of translational to rotational energy is also consistent with the QCT predictions of Troya on a fluorinated SAM surface, expected to be a reasonable model for PFPE, at the somewhat higher collision energy of our earlier experiments.[44-45, 82] The somewhat higher rotational temperature for squalene has also been seen by us previously, for which we have offered a potential explanation based on differential survival probabilities of hotter, less thermally accommodated molecules.[15-16] We return to this below in the context of our new measurements here of the collision-energy dependence of this survival.

The current measurements are probably not able to distinguish unambiguously between contributions from TD and IS scattering at the only modestly superthermal collision energy of $<E_k>$ = 7.20 kJ mol^{-1}. The product rotational temperatures are close to thermal and the TOF profiles also appear to be quite closely matched by a simulated TD profile. However, there are

some residual subtle differences in these profiles as a function of *N*, which are consistent with some contribution from an IS mechanism.

Survival Probabilities

At both collision energies studied in this paper, the survival probabilities are in the sequence PFPE > squalane > squalene. (The assumption that the survival probability on PFPE is essentially unity is supported by our modeling of the relative magnitude of in-going and scattered signals, as noted above and described in Section 5 of the Supporting Information.) However, although the qualitative sequence remains the same, there is a clear *increase* in the survival probability from squalene at 29.5 kJ mol^{-1} relative to 7.20 kJ mol^{-1}. This trend is continued in the uptake of the previous photolytically generated OH at $\langle E_k \rangle$ = 54 kJ mol^{-1}. This is the first direct evidence that the sticking of OH (or OD) at the squalene surface is negatively activated. It suggests that the higher uptake on squalene than on squalane at lower collision energies is not simply the result of the lower activation energies to be expected for H-abstraction from the allylic C-H bonds in squalene.[43] Rather, it strongly reinforces the previous conclusion[15] that the higher uptake on squalene than on squalane at the single, higher translational energy was due to the existence of the extra channel of addition at the double-bond sites, to generate a transient hydroxyalkyl radical. This additional loss mechanism at the squalene surface is found in the current work to be significantly enhanced at the successively lower collision energies. This explanation is consistent with the analogous reactions of OH with alkenes in the gas phase, where the negatively activated addition mechanism is found to dominate for larger alkenes.[83] Even in smaller alkenes, studies on the branching ratio between H abstraction and addition reactions suggest that the latter predominate.[84]

In contrast, there is little evidence for any collision-energy dependence of the sticking of OD at the squalane surface. This is at first sight surprising, given that unambiguously the only reaction

channel available at these collision energies is direct abstraction of an H atom to form H_2O and an alkyl radical.[85] There is overwhelming evidence that this is a positively activated process for alkanes in the gas phase.[83, 85] However, the quantitative variation in reactivity that might be expected here obviously depends on the relationship between the collision energies spanned and the barrier heights. This is complicated by the presence of primary, secondary and tertiary sites in the squalane molecule, with significantly different bond strengths and corresponding activation energies.[86-87] More fundamentally, for all three C-H bond types the barriers are relatively low, below ~ 10 kJ mol^{-1}; Arrhenius plots are found to be strongly curved over the accessible range of temperatures for which they have been measured (typically 300 – 1200 K) for related alkane molecules in the gas phase.[86-87] As expressed in the Tolman interpretation,[88] it is not sufficient to therefore simply equate the Arrhenius activation energy, E_a, measured in any particular temperature range to the threshold energy, E_0. To proceed to a reasonable estimate of E_0 for the different C-H bond types in squalane, we have extrapolated from the relationship between E_a and E_0 for the well-studied parent molecule, ethane. E_a has been extensively measured for ethane,[83, 85] with broad agreement that the experimental value at temperatures in the vicinity of 300 K is around 8.9 kJ mol^{-1}. Sophisticated transition-state theory calculations, which incorporate the other temperature-dependent factors responsible for the curvature in Arrhenius plots, have shown that the experimental rate constants can be reproduced faithfully over the full measured range (200 - 1250 K) based on a zero-point-energy-corrected barrier height of 6.7 kJ mol^{-1}.[89] In the absence of equivalent detailed information, we make the assumption that a similar ratio between empirical, room-temperature E_a and threshold energies E_0 also applies to larger alkanes. Site-specific E_a values are available for a range of alkanes; we have selected the largest molecules for which data are available in which the abstraction takes place either exclusively or

predominantly around room temperature from a single C-H bond type. These E_a values are collected in Table 3, along with the projected values of E_0.

Table 3: Measured Arrhenius activation energies, E_a, around 300 K for gas-phase reactions of OH with different C-H bond types in alkanes and corresponding estimated threshold energies, E_0.

alkane	$\boldsymbol{E_a}$ **/ kJmol^{-1} (d)**	$\boldsymbol{E_0}$ **/ kJmol^{-1}**
ethane	8.9	6.7(e)
Large primary a)	7.6	5.8 (f)
Large secondary b)	3.4	2.5 (f)
Large tertiary c)	2.1	1.6 (f)

a) based on neopentane; b) based on cyclohexane; c) based on an average of 2,3-dimethylbutane and 2,3,4-trimethyl pentane; d) From reference [85]; (e) from reference [89]; (f) as estimated here by analogy with ethane, as described in the text.

A further requirement to assess how the reactivity might be expected to vary across the range of translational energies probed in our gas-liquid scattering experiments is to relate the laboratory-frame kinetic energies, $\langle E_k \rangle$, to center-of-mass collision energies, E_{coll}. It is well known from previous gas-liquid scattering experiments, and related studies at SAM surfaces, that

the surface behaves as if it has a finite mass, m_S.[30, 48-49, 81, 90-95] This is generally significantly less than the mass of an intact liquid molecule, including squalane as a specific well-studied example.[30, 92-94] E_{coll} and $\langle E_k \rangle$ are related by the simple expression

$$E_{coll} = \frac{m_s}{m_s + m_{OD}} \langle E_k \rangle \qquad (3)$$

where m_{OD} is the mass of OD. There are no previous experiments on OH (or OD) scattering from squalane surfaces from which we can adopt a value for m_S. However, there have been a number of studies by Minton and coworkers on O(^{3}P) atom scattering from squalane surfaces.[30, 92-94] They find that m_S generally has an inverse dependence on collision energy, for well understood reasons. For the lowest lab-frame energies, $\langle E_k \rangle$ = 47 kJ mol^{-1}, for which results are available for O + squalane collisions, they report m_S = 109 amu for inelastic scattering of O and 76 amu for reactive scattering to form OH. We would expect OH (or OD) to be reasonably kinematically similar to scattering of O(^{3}P) from squalane and so adopt an indicative value of m_S = 100 amu. (The conclusions towards which we are proceeding are not significantly altered by the precise value assumed.)

On this basis, for the two $\langle E_k \rangle$ values studied here of 7.20 ± 0.06 and 29.5 ± 0.3 kJ mol^{-1}, E_{coll} is estimated to be around 6.10 ± 0.05 and 25.0 ± 0.2 kJ mol^{-1}, respectively. It is immediately obvious from inspection of Table 3 that collisions at the lower energy only modestly exceed the estimated E_0 values for secondary and tertiary C-H bonds, but are barely above threshold for primary C-H bonds. It is known from our own previous analysis of molecular dynamics simulations that the outer surface of squalane is occupied by primary, secondary and tertiary C-H sites in the ratio 0.41:0.50:0.09 (which is only slightly different from their stoichiometric ratios 0.39:0.51:0.10 in the squalane molecule).[37] Therefore, the important conclusion that we reach is that of order half of the exposed squalane surface should be unreactive to OD at the lower E_{coll}.

However, these sites should become substantially more reactive at the higher E_{coll}, which exceeds the threshold energy by an estimated factor of more than 4. If we were to assume, again for the purposes of illustration, that the excitation function was reasonably well described by the simple but physically realistic line-of-centers model expression[96]

$$\sigma = \sigma_{\max}\left(1 - \frac{E_0}{E_{coll}}\right) \qquad (4)$$

where σ_{max} is the asymptotic high-energy value of the reaction cross section, σ, then the reactivity of the primary C-H sites should have reached 74 % of σ_{max} at E_{coll} = 25.0 kJ mol^{-1}. If a similar assumption is made that the excitation functions for the secondary and tertiary sites also resemble Equation (4), then the overall increase in the reactivity between Ne and He carrier experiments is predicted to be more than a factor of 2, as shown in detail in the Supporting Information (Section 6).

As we wish to emphasize, however, there is no sign of such a strong decline in the measured survival probabilities as a function of collision energy in Table 2; within the experimental uncertainty, the survival coefficients are essentially the same at around 65% for both collision energies here. There are undoubtedly some detailed differences in incident angular distributions and possibly in the sampling of the product angular distributions between the current experiments and the previous higher-energy photolytic experiments.[14-15] Some caution should also be exercised when comparing experiments with different incident rotational distributions; these vary subtly between the He and Ne carriers here, as characterized above, but more significantly in the photolytic experiments. Any rotational-level dependence of the sticking coefficients could therefore, in principle, independently affect the overall uptake. Nevertheless, regardless of the possible influence of these effects, the result in the photolytic experiments continues the essentially flat trend of the lower two collision energies. This is the sense in which

we believe these results are surprising, and for which some alternative explanation must be sought.

One interesting such possibility is that the expected reduced reactivity in direct, IS-like trajectories is compensated by an increase in the proportion that undergo TD-like accommodation at the squalane surface. If these accommodated molecules are able to migrate until they encounter a more reactive secondary or especially tertiary C-H site, they will have an enhanced probability of reaction. This is in some ways analogous to the switch between the well-known 'Eley-Rideal' and 'Langmuir-Hinshelwood' mechanisms in heterogeneous reactions catalysed by solid surfaces. It would be consistent with those molecules that do escape the squalane surface retaining some of the characteristics of IS trajectories even at lower collision energies, including a positive correlation between translational and rotational energies. As noted above, this effect would be even more amplified in reaction at the *squalene* surface at the higher collision energies, where OH molecules which have been accommodated at the surface have a strongly enhanced probability of undergoing an addition reaction at a double-bond site. Although the differences are modest relative to the experimental uncertainties, it is interesting that the observed OD or OH rotational temperatures from scattering from squalene at $<E_k>$ here of 29.5 kJ mol^{-1} or previously of 54 kJ mol^{-1} are consistently higher than those from squalane and more similar to those from PFPE, despite its known 'stiffer' surface. This would be compatible with only the most direct, impulsively scattered OH molecules escaping from squalene, whereas this constraint is weaker in squalane.

This work therefore has potentially important consequences for the understanding and modeling of OH uptake on atmospheric aerosol surfaces. The fact that we have demonstrated that the collision-energy dependence is strongly affected by the chemical nature of the surface

implies that the corresponding temperature dependence of uptake in the atmosphere is almost certainly a non-trivial function of the initial and evolving composition of the aerosol surface during ageing. Furthermore, even for surfaces of a known composition, we have shown that both the absolute values and the temperature dependence of OH uptake may not simply reflect the behavior that would be expected on the basis of extrapolation from the corresponding gas-phase reactions. Our previous result for primary uptake on squalane, in particular, has been invoked by others in an atmospheric context.[11, 58] However, although this may be entirely reasonable because it was the best value available, it might not have been secure because it was measured at the much higher collision energies of our previous photolytic experiments; these are not characteristic of ambient atmospheric conditions. Reassuringly, among the interesting results here is the observation, regardless of its explanation, that the sticking coefficient on squalane actually remains almost constant (at a value of ~0.35) as the collision energy is reduced to more nearly thermal collision energies.

Conclusions

A new, molecular-beam-based approach to the measurement of collision-energy-dependent sticking coefficients of hydroxyl radicals (in practice, OD) at model involatile liquid surfaces has been demonstrated successfully. As expected, OD uptake on the partially unsaturated squalene surface is found to be negatively activated. More surprisingly, the positively activated behavior expected for squalane on the basis of analogous OH + alkane gas-phase reactions is not observed. We speculate that this may be the result of trapping-enhanced reactivity at lower collision energies.

ASSOCIATED CONTENT

Supporting Information.

Section 1, incident beam flux versus density of surface sites; Section 2, characterization of the incident beam; Section 3, rotational temperatures obtained from excitation spectra; Section 4, global rotational temperatures extracted from a Boltzmann analysis of the integrated scattered OD TOF profiles; Section 5, testing the assumption that OD is not lost on the surface by any other process; Section 6, E_{coll} dependence of sticking based on model excitation functions. This material is available free of charge via the Internet at http://pubs.acs.org.

AUTHOR INFORMATION

Corresponding Author

*E-mail: k.g.mckendrick@hw.ac.uk.

Funding Sources

EPSRC (grant numbers EP/G029601/1, EP/P001459/1).

Heriot-Watt University.

Notes

All data created during this research are available by request from the Heriot-Watt University data repository.

ACKNOWLEDGMENT

The authors acknowledge financial support from EPSRC (grant numbers EP/G029601/1, EP/P001459/1) and Heriot-Watt University (James Watt Scholarships to RHB and MAT-S). We are grateful to Paul Bagot, Grant Paterson and Matthew Bain for contributions to the development of the apparatus, to Stuart Greaves for providing the electric-discharge device used and to Paul Lane for assistance with optimizing its performance, and to Mira Rupp for assistance with some of the measurements.

REFERENCES

(1) Heard, D. E.; Pilling, M. J., Measurement of OH and HO_2 in the troposphere. *Chem. Rev.* **2003,** *103* (12), 5163-5198.
(2) Finlayson, P.; Pitts, *Chemistry of the upper and lower atmosphere : theory, experiments, and applications*. Academic P.: Cambridge, MA, 2000.
(3) Finlayson-Pitts, B. J., Reactions at surfaces in the atmosphere: integration of experiments and theory as necessary (but not necessarily sufficient) for predicting the physical chemistry of aerosols. *Phys. Chem. Chem. Phys.* **2009,** *11* (36), 7760-7779.
(4) Rudich, Y., Laboratory perspectives on the chemical transformations of organic matter in atmospheric particles. *Chem. Rev.* **2003,** *103* (12), 5097-5124.
(5) Ellison, G. B.; Tuck, A. F.; Vaida, V., Atmospheric processing of organic aerosols. *J. Geophys. Res.: Atmos.* **1999,** *104* (D9), 11633-11641.
(6) Donaldson, D. J.; Vaida, V., The influence of organic films at the air-aqueous boundary on atmospheric processes. *Chem. Rev.* **2006,** *106* (4), 1445-1461.
(7) Enami, S.; Sakamoto, Y.; Hara, K.; Osada, K.; Hoffmann, M. R.; Colussi, A. J., "Sizing" heterogeneous chemistry in the conversion of gaseous dimethyl sulfide to atmospheric particles. *Environ. Sci. Technol.* **2016,** *50* (4), 1834-1843.
(8) Chapleski, R. C.; Zhang, Y.; Troya, D.; Morris, J. R., Heterogeneous chemistry and reaction dynamics of the atmospheric oxidants, O_3, NO_3, and OH, on organic surfaces. *Chem. Soc. Rev.* **2016**.
(9) Enami, S.; Hoffmann, M. R.; Colussi, A. J., OH-radical specific addition to glutathione S-atom at the air-water interface: Relevance to the redox balance of the lung epithelial lining fluid. *J. Phys. Chem. Lett.* **2015,** *6* (19), 3935-3943.
(10) Crowley, J. N.; Ammann, M.; Cox, R. A.; Hynes, R. G.; Jenkin, M. E.; Mellouki, A.; Rossi, M. J.; Troe, J.; Wallington, T. J., Evaluated kinetic and photochemical data for

atmospheric chemistry: Volume V - heterogeneous reactions on solid substrates. *Atmos. Chem. Phys.* **2010,** *10* (18), 9059-9223.
(11) Houle, F. A.; Hinsberg, W. D.; Wilson, K. R., Oxidation of a model alkane aerosol by OH radical: the emergent nature of reactive uptake. *Phys. Chem. Chem. Phys.* **2015,** *17* (6), 4412-4423.
(12) Bertram, A. K.; Ivanov, A. V.; Hunter, M.; Molina, L. T.; Molina, M. J., The reaction probability of OH on organic surfaces of tropospheric interest. *J. Phys. Chem. A* **2001,** *105* (41), 9415-9421.
(13) Park, J.-H.; Ivanov, A. V.; Molina, M. J., Effect of relative humidity on OH uptake by surfaces of atmospheric importance. *J. Phys. Chem. A* **2008,** *112* (30), 6968-6977.
(14) Bagot, P. A. J.; Waring, C.; Costen, M. L.; McKendrick, K. G., Dynamics of inelastic scattering of OH radicals from reactive and inert liquid surfaces. *J. Phys. Chem. C* **2008,** *112* (29), 10868-10877.
(15) Waring, C.; King, K. L.; Bagot, P. A. J.; Costen, M. L.; McKendrick, K. G., Collision dynamics and reactive uptake of OH radicals at liquid surfaces of atmospheric interest. *Phys. Chem. Chem. Phys.* **2011,** *13* (18), 8457-8469.
(16) King, K. L.; Paterson, G.; Rossi, G. E.; Iljina, M.; Westacott, R. E.; Costen, M. L.; McKendrick, K. G., Inelastic scattering of OH radicals from organic liquids: isolating the thermal desorption channel. *Phys. Chem. Chem. Phys.* **2013,** *15* (31), 12852-12863.
(17) Molina, M. J.; Ivanov, A. V.; Trakhtenberg, S.; Molina, L. T., Atmospheric evolution of organic aerosol. *Geophys. Res. Lett.* **2004,** *31* (22), 5.
(18) Slade, J. H.; Knopf, D. A., Heterogeneous OH oxidation of biomass burning organic aerosol surrogate compounds: assessment of volatilisation products and the role of OH concentration on the reactive uptake kinetics. *Phys. Chem. Chem. Phys.* **2013,** *15* (16), 5898-5915.
(19) Cooper, P. L.; Abbatt, J. P. D., Heterogeneous interactions of OH and HO_2 radicals with surfaces characteristic of atmospheric particulate matter. *J. Phys. Chem.* **1996,** *100* (6), 2249-2254.
(20) George, I. J.; Abbatt, J. P. D., Heterogeneous oxidation of atmospheric aerosol particles by gas-phase radicals. *Nature Chem.* **2010,** *2* (9), 713-722.
(21) Moussa, S. G.; Finlayson-Pitts, B. J., Reaction of gas phase OH with unsaturated self-assembled monolayers and relevance to atmospheric organic oxidations. *Phys. Chem. Chem. Phys.* **2010,** *12* (32), 9419-9428.
(22) Hearn, J. D.; Smith, G. D., A mixed-phase relative rates technique for measuring aerosol reaction kinetics. *Geophys. Res. Lett.* **2006,** *33* (17).
(23) Che, D. L.; Smith, J. D.; Leone, S. R.; Ahmed, M.; Wilson, K. R., Quantifying the reactive uptake of OH by organic aerosols in a continuous flow stirred tank reactor. *Phys. Chem. Chem. Phys.* **2009,** *11* (36), 7885-7895.
(24) Lambe, A. T.; Zhang, J.; Sage, A. M.; Donahue, N. M., Controlled OH radical production via ozone-alkene reactions for use in aerosol aging studies. *Environ. Sci. Technol.* **2007,** *41* (7), 2357-2363.
(25) McNeill, V. F.; Yatavelli, R. L. N.; Thornton, J. A.; Stipe, C. B.; Landgrebe, O., Heterogeneous OH oxidation of palmitic acid in single component and internally mixed aerosol particles: vaporization and the role of particle phase. *Atmos. Chem. Phys.* **2008,** *8* (17), 5465-5476.

(26) Park, J. H.; Christov, C. I.; Ivanov, A. V.; Molina, M. J., On OH uptake by sea salt under humid conditions. *Geophys. Res. Lett.* **2009,** *36*, 5.
(27) Enami, S.; Hoffmann, M. R.; Colussi, A. J., In situ mass spectrometric detection of interfacial intermediates in the oxidation of RCOOH(aq) by gas-phase OH-radicals. *J. Phys. Chem. A* **2014,** *118* (23), 4130-4137.
(28) Tesa-Serrate, M. A.; Smoll, E. J.; Minton, T. K.; McKendrick, K. G., Atomic and molecular collisions at liquid surfaces. In *Annu. Rev. Phys. Chem.*, Johnson, M. A.; Martinez, T. J., Eds. Annual Reviews: Palo Alto, 2016; Vol. 67, pp 515-540.
(29) Nathanson, G. M., Molecular beam studies of gas-liquid interfaces. *Annu. Rev. Phys. Chem.* **2004,** *55*, 231-255.
(30) Garton, D. J.; Minton, T. K.; Alagia, M.; Balucani, N.; Casavecchia, P.; Volpi, G. G., Reactive scattering of ground-state and electronically excited oxygen atoms on a liquid hydrocarbon surface. *Faraday Discuss.* **1997,** *108*, 387-399.
(31) Kenyon, A. J.; McCaffery, A. J.; Quintella, C. M.; Zidan, M. D., Dynamics of the gas-liquid interface from laser molecular-beam scattering. *Faraday Discuss.* **1993,** *96*, 245-254.
(32) Kenyon, A. J.; McCaffery, A. J.; Quintella, C. M.; Zidan, M. D., Investigation of dynamical processes at liquid surfaces by molecular-scattering. *J. Chem. Soc. Faraday Trans.* **1993,** *89* (21), 3877-3884.
(33) Ausfelder, F.; McKendrick, K. G., The dynamics of reactions of $O(^3P)$ atoms with saturated hydrocarbons and related compounds. *Prog. React. Kinet. Mech.* **2000,** *25* (4), 299-370.
(34) Kelso, H.; Kohler, S. P. K.; Henderson, D. A.; McKendrick, K. G., Dynamics of the gas-liquid interfacial reaction of $O(^3P)$ atoms with hydrocarbons. *J. Chem. Phys.* **2003,** *119* (19), 9985-9988.
(35) Kohler, S. P. K.; Allan, M.; Kelso, H.; Henderson, D. A.; McKendrick, K. G., The effects of surface temperature on the gas-liquid interfacial reaction dynamics of $O(^3P)$ plus squalane. *J. Chem. Phys.* **2005,** *122* (2).
(36) Kohler, S. P. K.; Allan, M.; Costen, M. L.; McKendrick, K. G., Direct gas-liquid interfacial dynamics: The reaction between $O(^3P)$ and a liquid hydrocarbon. *J. Phys. Chem. B* **2006,** *110* (6), 2771-2776.
(37) Kohler, S. P. K.; Reed, S. K.; Westacott, R. E.; McKendrick, K. G., Molecular dynamics study to identify the reactive sites of a liquid squalane surface. *J. Phys. Chem. B* **2006,** *110* (24), 11717-11724.
(38) Allan, M.; Bagot, P. A. J.; Koehler, S. P. K.; Reed, S. K.; Westacott, R. E.; Costen, M. L.; McKendrick, K. G., Dynamics of interfacial reactions between $O(^3P)$ atoms and long-chain liquid hydrocarbons. *Phys. Scr.* **2007,** *76* (3), C42-C47.
(39) Allan, M.; Bagot, P. A. J.; Costen, M. L.; McKendrick, K. G., Temperature dependence of OH yield, translational energy, and vibrational branching in the reaction of $O(^3P)$(g) with liquid squalane. *J. Phys. Chem. C* **2007,** *111* (40), 14833-14842.
(40) Allan, M.; Bagot, P. A. J.; Westacott, R. E.; Costen, M. L.; McKendrick, K. G., Influence of molecular and supramolecular structure on the gas-liquid interfacial reactivity of hydrocarbon liquids with $O(^3P)$ atoms. *J. Phys. Chem. C* **2008,** *112* (5), 1524-1532.
(41) Waring, C.; King, K. L.; Costen, M. L.; McKendrick, K. G., Dynamics of the gas-liquid interfacial reaction of $O(^1D)$ with a liquid hydrocarbon. *J. Phys. Chem. A* **2011,** *115* (25), 7210-7219.
(42) Waring, C.; Bagot, P. A. J.; Costen, M. L.; McKendrick, K. G., Reactive scattering as a chemically specific analytical probe of liquid surfaces. *J. Phys. Chem. Lett.* **2011,** *2* (1), 12-18.

(43) Tesa-Serrate, M. A.; King, K. L.; Paterson, G.; Costen, M. L.; McKendrick, K. G., Site and bond-specific dynamics of reactions at the gas-liquid interface. *Phys. Chem. Chem. Phys.* **2014,** *16* (1), 173-183.
(44) Waring, C.; Bagot, P. A. J.; Raeisaenen, M. T.; Costen, M. L.; McKendrick, K. G., Dynamics of the reaction of O(^{3}P) atoms with alkylthiol self-assembled monolayers. *J. Phys. Chem. A* **2009,** *113* (16), 4320-4329.
(45) Waring, C.; Bagot, P. A. J.; Bebbington, M. W. P.; Raisanen, M. T.; Buck, M.; Costen, M. L.; McKendrick, K. G., How penetrable are thioalkyl self-assembled monolayers? *J. Phys. Chem. Lett.* **2010,** *1* (13), 1917-1921.
(46) Waring, C.; Bagot, P. A. J.; Slattery, J. M.; Costen, M. L.; McKendrick, K. G., O(^{3}P) atoms as a chemical probe of surface ordering in ionic liquids. *J. Phys. Chem. A* **2010,** *114* (14), 4896-4904.
(47) Waring, C.; Bagot, P. A. J.; Slattery, J. M.; Costen, M. L.; McKendrick, K. G., O(^{3}P) atoms as a probe of surface ordering in 1-alkyl-3-methylimidazolium-based ionic liquids. *J. Phys. Chem. Lett.* **2010,** *1* (1), 429-433.
(48) Wu, B.; Zhang, J.; Minton, T. K.; McKendrick, K. G.; Slattery, J. M.; Yockel, S.; Schatz, G. C., Scattering dynamics of hyperthermal oxygen atoms on ionic liquid surfaces: [emim][NTf_2] and [C_{12}mim][NTf_2]. *J. Phys. Chem. C* **2010,** *114* (9), 4015-4027.
(49) Tesa-Serrate, M. A.; Marshall, B. C.; Smoll, E. J.; Purcell, S. M.; Costen, M. L.; Slattery, J. M.; Minton, T. K.; McKendrick, K. G., Ionic liquid-vacuum interfaces probed by Reactive Atom Scattering: influence of alkyl chain length and anion volume. *J. Phys. Chem. C* **2015,** *119* (10), 5491-5505.
(50) Ziemkiewich, M. P.; Zutz, A.; Nesbitt, D. J., Inelastic scattering of radicals at the gas-ionic liquid interface: probing surface dynamics of BMIM-Cl, BMIM-BF_4, and BMIM-Tf_2N by rovibronic scattering of NO [$^2\Pi_{1/2}$(0.5)]. *J. Phys. Chem. C* **2012,** *116* (27), 14284-14294.
(51) Zutz, A.; Nesbitt, D. J., Angle-resolved molecular beam scattering of NO at the gas-liquid interface. *J. Chem. Phys.* **2017,** *147* (5), 12.
(52) Perkins, B. G.; Haber, T.; Nesbitt, D. J., Quantum state-resolved energy transfer dynamics at gas-liquid interfaces: IR laser studies of CO_2 scattering from perfluorinated liquids. *J. Phys. Chem. B* **2005,** *109* (34), 16396-16405.
(53) Nogueira, J. J.; Vazquez, S. A.; Mazyar, O. A.; Hase, W. L.; Perkins, B. G., Jr.; Nesbitt, D. J.; Martinez-Nunez, E., Dynamics of CO_2 scattering off a perfluorinated self-assembled monolayer. Influence of the incident collision energy, mass effects, and use of different surface models. *J. Phys. Chem. A* **2009,** *113* (16), 3850-3865.
(54) Perkins, B. G.; Nesbitt, D. J., High resolution Dopplerimetry of correlated angular and quantum state-resolved CO_2 scattering dynamics at the gas-liquid interface. *Phys. Chem. Chem. Phys.* **2010,** *12* (42), 14294-14308.
(55) Perkins, B. G.; Nesbitt, D. J., Stereodynamics at the gas-liquid interface: orientation and alignment of CO_2 scattered from perfluorinated liquid surfaces. *J. Phys. Chem. A* **2010,** *114* (3), 1398-1410.
(56) Zolot, A. M.; Harper, W. W.; Perkins, B. G.; Dagdigian, P. J.; Nesbitt, D. J., Quantum-state resolved reaction dynamics at the gas-liquid interface: Direct absorption detection of HF(*v,J*) product from F(^{2}P) + squalane. *J. Chem. Phys.* **2006,** *125* (2).
(57) Zolot, A. M.; Dagdigian, P. J.; Nesbitt, D. J., Quantum-state resolved reactive scattering at the gas-liquid interface: F + squalane ($C_{30}H_{62}$) dynamics via high-resolution infrared absorption of nascent HF(*v,J*). *J. Chem. Phys.* **2008,** *129* (19), 11.

(58) Lu, J. W.; Day, B. S.; Fiegland, L. R.; Davis, E. D.; Alexander, W. A.; Troya, D.; Morris, J. R., Interfacial energy exchange and reaction dynamics in collisions of gases on model organic surfaces. *Prog. Surf. Sci.* **2012,** *87* (9-12), 221-252.
(59) Yockel, S.; Schatz, G. C., Modeling O(^{3}P) and Ar scattering from the ionic liquid [emim][NO_3] at 5 eV with hybrid QM/MM Molecular Dynamics. *J. Phys. Chem. B* **2010,** *114* (45), 14241-14248.
(60) Tasic, U. S.; Yan, T. Y.; Hase, W. L., Dynamics of energy transfer in collisions of O(^{3}P) atoms with a 1-decanethiol self-assembled monolayer surface. *J. Phys. Chem. B* **2006,** *110* (24), 11863-11877.
(61) Martinez-Nunez, E.; Rahaman, A.; Hase, W. L., Chemical dynamics Simulations of CO_2 scattering off a fluorinated self-assembled monolayer surface. *J. Phys. Chem. C* **2007,** *111* (1), 354-364.
(62) Vazquez, S. A.; Morris, J. R.; Rahaman, A.; Mazyar, O. A.; Vayner, G.; Addepalli, S. V.; Hase, W. L.; Martinez-Nunez, E., Inelastic scattering dynamics of Ar from a perfluorinated self-assembled monolayer surface. *J. Phys. Chem. A* **2007,** *111* (49), 12785-12794.
(63) Troya, D.; Schatz, G. C., Theoretical studies of hyperthermal O(^{3}P) collisions with hydrocarbon self-assembled monolayers. *J. Chem. Phys.* **2004,** *120* (16), 7696-7707.
(64) Dhanya, S.; Kumar, A.; Upadhyaya, H. P.; Naik, P. D.; Saini, R. D., Photodissociation of unsaturated alcohols. Energy distribution in the nascent OH radicals. *J. Phys. Chem. A* **2004,** *108* (38), 7646-7652.
(65) Kang, T. Y.; Shin, S. K.; Kim, H. L., Photodissociation dynamics of allyl alcohol at 193 nm. *J. Phys. Chem. A* **2003,** *107* (50), 10888-10892.
(66) van Beek, M. C.; ter Meulen, J. J., An intense pulsed electrical discharge source for OH molecular beams. *Chem. Phys. Lett.* **2001,** *337* (4-6), 237-242.
(67) Ikejiri, K.; Ohoyama, H.; Nagamachi, Y.; Teramoto, T.; Kasai, T., A highly intense state-selected OH beam source by the pulsed electric DC discharge method. *Chem. Phys. Lett.* **2003,** *379* (3-4), 255-260.
(68) Lewandowski, H. J.; Hudson, E. R.; Bochinski, J. R.; Ye, J., A pulsed, low-temperature beam of supersonically cooled free radical OH molecules. *Chem. Phys. Lett.* **2004,** *395* (1-3), 53-57.
(69) Ploenes, L.; Haas, D.; Zhang, D. D.; van de Meerakker, S. Y. T.; Willitsch, S., Cold and intense OH radical beam sources. *Rev. Sci. Instrum.* **2016,** *87* (5), 6.
(70) Davis, S.; Anderson, D. T.; Duxbury, G.; Nesbitt, D. J., Jet-cooled molecular radicals in slit supersonic discharges: Sub-Doppler infrared studies of methyl radical. *J. Chem. Phys.* **1997,** *107* (15), 5661-5675.
(71) Yan, B.; Claus, P. F. H.; van Oorschot, B. G. M.; Gerritsen, L.; Eppink, A.; van de Meerakker, S. Y. T.; Parker, D. H., A new high intensity and short-pulse molecular beam valve. *Rev. Sci. Instrum.* **2013,** *84* (2), 8.
(72) Scoles, G., *Atomic and molecular beam methods* OUP: New York, 1988; Vol. 1.
(73) Saecker, M. E.; Nathanson, G. M., Collisions of protic and aprotic gases with hydrogen-bonding and hydrocarbon liquids. *J. Chem. Phys.* **1993,** *99* (9), 7056-7075.
(74) Brastad, S. M.; Nathanson, G. M., Molecular beam studies of HCl dissolution and dissociation in cold salty water. *Phys. Chem. Chem. Phys.* **2011,** *13* (18), 8284-8295.
(75) Johansson, S. M.; Kong, X. R.; Thomson, E. S.; Hallquist, M.; Pettersson, J. B. C., The dynamics and kinetics of water interactions with a condensed nopinone surface. *J. Phys. Chem. A* **2017,** *121* (35), 6614-6619.

(76) Ohno, K.; Takami, T.; Mitsuke, K.; Ishida, T., State-resolved collision energy-dependence of Penning ionization cross-sections for N_2 and CO_2 by He*2^3S. *J. Chem. Phys.* **1991,** *94* (4), 2675-2687.
(77) Halfmann, T.; Koensgen, J.; Bergmann, K., A source for a high-intensity pulsed beam of metastable helium atoms. *Meas. Sci. Technol.* **2000,** *11* (10), 1510-1514.
(78) Feng, P. X.; Weiner, B., A collimated pulsed supersonic metastable helium atomic beam. *Phys. Scr.* **2007,** *75* (4), 565-571.
(79) Harris, K. R., Viscous calibration liquids for self-diffusion measurements. *J. Chem. Eng. Data* **2015,** *60* (12), 3506-3517.
(80) Luque, J.; Crosley, D. R. *LIFBASE: Database and spectral simulation for diatomic molecules*, Version 1.5; SRI International: 1999.
(81) Alexander, W. A.; Zhang, J.; Murray, V. J.; Nathanson, G. M.; Minton, T. K., Kinematics and dynamics of atomic-beam scattering on liquid and self-assembled monolayer surfaces. *Faraday Discuss.* **2012,** *157*, 355-374.
(82) Troya, D., Dynamics of collisions of hydroxyl radicals with fluorinated self-assembled monolayers. *Theor. Chem. Acc.* **2012,** *131* (1).
(83) Atkinson, R.; Arey, J., Atmospheric degradation of volatile organic compounds. *Chem. Rev.* **2003,** *103* (12), 4605-4638.
(84) Loison, J. C.; Daranlot, J.; Bergeat, A.; Caralp, F.; Mereau, R.; Hickson, K. M., Gas-phase kinetics of hydroxyl radical reactions with C_3H_6 and C_4H_8: product branching ratios and OH addition site-specificity. *J. Phys. Chem. A* **2010,** *114* (51), 13326-13336.
(85) Wilson, E. W.; Hamilton, W. A.; Kennington, H. R.; Evans, B.; Scott, N. W.; DeMore, W. B., Measurement and estimation of rate constants for the reactions of hydroxyl radical with several alkanes and cycloalkanes. *J. Phys. Chem. A* **2006,** *110* (10), 3593-3604.
(86) Badra, J.; Farooq, A., Site-specific reaction rate constant measurements for various secondary and tertiary H-abstraction by OH radicals. *Combust. Flame* **2015,** *162* (5), 2034-2044.
(87) Liu, D. P.; Khaled, F.; Giri, B. R.; Assaf, E.; Fittschen, C.; Farooq, A., H-abstraction by OH from large branched alkanes: Overall rate measurements and site-specific tertiary rate calculations. *J. Phys. Chem. A* **2017,** *121* (5), 927-937.
(88) Laidler, K. J., *Chemical Kinetics*. 3rd edition ed.; Harper & Row: New York, 1987.
(89) Diamanti, A.; Adjiman, C. S.; Piccione, P. M.; Rea, A. M.; Galindo, A., Development of predictive models of the kinetics of a hydrogen abstraction reaction combining Quantum-Mechanical calculations and experimental data. *Ind. Eng. Chem. Res.* **2017,** *56* (4), 815-831.
(90) King, M. E.; Nathanson, G. M.; Hanninglee, M. A.; Minton, T. K., Probing the microscopic corrugation of liquid surfaces with gas-liquid collisions. *Phys. Rev. Lett.* **1993,** *70* (7), 1026-1029.
(91) King, M. E.; Fiehrer, K. M.; Nathanson, G. M.; Minton, T. K., Effects of thermal roughening on the angular distributions of trapping and scattering in gas-liquid collisions. *J. Phys. Chem. A* **1997,** *101* (36), 6556-6561.
(92) Garton, D. J.; Minton, T. K.; Alagia, M.; Balucani, N.; Casavecchia, P.; Volpi, G. G., Comparative dynamics of Cl(^{2}P) and O(^{3}P) interactions with a hydrocarbon surface. *J. Chem. Phys.* **2000,** *112* (13), 5975-5984.
(93) Zhang, J. M.; Garton, D. J.; Minton, T. K., Reactive and inelastic scattering dynamics of hyperthermal oxygen atoms on a saturated hydrocarbon surface. *J. Chem. Phys.* **2002,** *117* (13), 6239-6251.

(94) Zhang, J. M.; Upadhyaya, H. P.; Brunsvold, A. L.; Minton, T. K., Hyperthermal reactions of O and O_2 with a hydrocarbon surface: Direct C-C bond breakage by O and H-atom abstraction by O_2. *J. Phys. Chem. B* **2006,** *110* (25), 12500-12511.
(95) Marshall, B. C.; Smoll, E. J.; Purcell, S. M.; Costen, M. L.; McKendrick, K. G.; Minton, T. K., Scattering dynamics of oxygen atoms on imidazolium tetrafluoroborate ionic liquid surfaces: Dependence on alkyl chain length. *J. Phys. Chem. C* **2016,** *120* (23), 12472-12483.
(96) Levine, R. D., *Molecular Reaction Dynamics*. Cambridge University Press: Cambridge, 2005.

ToC graphic

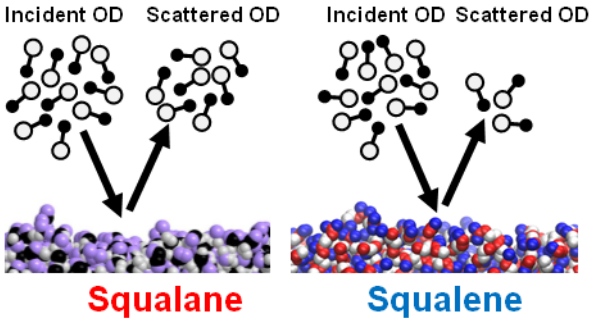

The collision-energy dependence of the uptake of hydroxyl radicals at liquid surfaces is highly sensitive to chemical composition.